ORIGINAL ARTICLE

^{68}Ga-PSMA-11 Dynamic PET/CT Imaging in Primary Prostate Cancer

Christos Sachpekidis, MD,† Klaus Kopka, PhD,‡ Matthias Eder, PhD,‡ Boris A. Hadaschik, MD,§ Martin T. Freitag, MD,|| Leyun Pan, PhD,* Uwe Haberkorn, MD,*¶ and Antonia Dimitrakopoulou-Strauss, MD**

Purpose: The aim of our study is to assess the pharmacokinetics and biodistribution of ^{68}Ga-PSMA-11 in patients suffering from primary prostate cancer (PC) by means of dynamic and whole-body PET/CT.

Materials and methods: Twenty-four patients with primary, previously untreated PC were enrolled in the study. All patients underwent dynamic PET/CT (dPET/CT) scanning of the pelvis and whole-body PET/CT studies with ^{68}Ga-PSMA-11. The evaluation of dPET/CT studies was based on qualitative evaluation, SUV calculation, and quantitative analysis based on two-tissue compartment modeling and a noncompartmental approach leading to the extraction of fractal dimension (FD).

Results: A total of 23/24 patients (95.8%) were ^{68}Ga-PSMA-11 positive. In 9/24 patients (37.5%), metastatic lesions were detected. PC-associated lesions demonstrated the following mean values: $SUV_{average}$ = 14.3, SUV_{max} = 23.4, K_1 = 0.24 (1/min), k_3 = 0.34 (1/min), influx = 0.15 (1/min), and FD = 1.27. The parameters $SUV_{average}$, SUV_{max}, k_3, influx, and FD derived from PC-associated lesions were significantly higher than respective values derived from reference prostate tissue. Time-activity curves derived from PC-associated lesions revealed an increasing ^{68}Ga-PSMA-11 accumulation during dynamic PET acquisition. Correlation analysis revealed a moderate but significant correlation between PSA levels and $SUV_{average}$ (r = 0.60) and SUV_{max} (r = 0.57), and a weak but significant correlation between Gleason score and $SUV_{average}$ (r = 0.33) and SUV_{max} (r = 0.28).

Conclusion: ^{68}Ga-PSMA-11 PET/CT confirmed its capacity in detecting primary PC with a detection rate of 95.8%. Dynamic PET/CT studies of the pelvis revealed an increase in tracer uptake in PC-associated lesions during the 60 minutes of dynamic PET acquisition, a finding with potential applications in anti-PSMA approaches.

Key Words: ^{68}Ga-PSMA-11 PET/CT, primary prostate cancer, two-tissue compartment model

(*Clin Nucl Med* 2016;41: e473–e479)

To date, the contribution of conventional imaging modalities in staging and management of men with prostate cancer (PC) is smaller than in other common cancers.[1–6] Imaging studies exhibit a low positivity in clinically localized disease (with the exception of patients with PSA levels ≥20 ng/mL or Gleason scores ≥8) and a low sensitivity in detecting lymph node metastases. With the exception of ^{18}F-choline and ^{11}C-acetate PET/CT, which demonstrated a high sensitivity in the biochemical relapse of PC,[7–9] the performance of most imaging approaches in detecting metastatic or recurrent PC in the setting of biochemical relapse is also not high.[4,10–14] Therefore, the development and introduction into clinical practice of new imaging modalities that carry high sensitivity and specificity in PC detection is of outmost importance.

The first results of the novel agent ^{68}Ga-labeled Glu-urea-Lys-(Ahx)-HBED-CC (^{68}Ga-PSMA-11) have been very satisfying, rendering the addition of ^{68}Ga-PSMA-11 PET/CT to the diagnostic armamentarium a very promising approach in PC staging.[10,15–17] This tracer carries some very desirable characteristics for the imaging approach of PC: specific targeting of prostate-specific membrane antigen (PSMA), fast blood clearance, low background activity, and a relative short physical half-life of the isotope (68.3 min).[18,19]

Dynamic PET/CT (dPET/CT) is a modality that allows registration of pharmacokinetic information over time, unlike classical whole-body PET/CT protocols that enable the acquisition of patient images only at one time point after tracer injection. Compartment analysis provides the possibility to assess dedicated aspects of tracer kinetics, which are associated with molecular biological data, and represents simplifications of actual complicated *in vivo* processes. In this sense, the two-tissue compartment model performed in the present study is an approximation of the underlying biological system regarding ^{68}Ga-PSMA-11 metabolism. The application of two-tissue compartment modeling in the ^{68}Ga-PSMA-11 dynamic PET data leads to the extraction of four transport rates (K_1, k_2, k_3, k_4), which describe the tracer exchange between plasma and tissue. In particular, K_1 and k_2 reflect the forward and reverse transport of the radiotracer between plasma and the reversible compartment, which involves free tracer in interstitial fluid. Respectively, k_3 and k_4 account for forward and reverse transport between the reversible and trapped compartment, which involves the PSMA-specific part of tracer metabolism, leading to the assumption that the constant rate k_3 is associated with tracer binding on the receptor (PSMA) and its internalization, and k_4 with dissociation of the tracer from the receptor and externalization.[20,21] This model has been used by our group for the pharmacokinetic analysis of ^{68}Ga-PSMA-11 studies in patients with biochemical relapse of PC.[20]

The aim of this study is to evaluate the biodistribution and pharmacokinetics of ^{68}Ga-PSMA-11 in patients with primary PC by means of dynamic and whole-body PET/CT. The correlation between PSA levels and ^{68}Ga-PSMA-11 PET parameters is also investigated.

PATIENTS AND METHODS

Patients

Twenty-four patients suffering from primary, previously untreated PC were enrolled in the study. Their median age was 69 years (range = 43–84 years). The median PSA value was 24.1 ng/mL (range = 3.2–200.0 ng/mL). Gleason score was available in 21/24 patients (median = 7; range = 7–9). Table 1 presents analytically the characteristics of the patients investigated. The analysis was conducted in accordance to the Declaration of Helsinki with institutional approval.

Received for publication April 19, 2016; revision accepted July 3, 2016.
From the *Clinical Cooperation Unit Nuclear Medicine, German Cancer Research Center (DKFZ), Heidelberg, Germany; †Department of Nuclear Medicine, Inselspital, Bern University Hospital, University of Bern, Bern, Switzerland; ‡Division of Radiopharmaceutical Chemistry, German Cancer Research Center (DKFZ), Heidelberg; §Department of Urology, University Hospital Heidelberg, Heidelberg; ||Department of Radiology, German Cancer Research Center (DKFZ), Heidelberg; and ¶Department of Nuclear Medicine, University of Heidelberg, Heidelberg, Germany.
Conflicts of interest and sources of funding: none declared.
Correspondence to: Christos Sachpekidis, MD, Medical PET Group—Biological Imaging, Clinical Cooperation Unit Nuclear Medicine, German Cancer Research Center, Im Neuenheimer Feld 280, D-69210 Heidelberg, Germany. E-mail: christos_saxpe@yahoo.gr.

ISSN: 0363-9762/16/4111–e473
DOI: 10.1097/RLU.0000000000001349

TABLE 1. Characteristics of the Patients Investigated in the Study

Patient No.	Age (y)	Dosage (MBq)	PSA (ng/mL)	Gleason Score	PC foci in the Prostate	Lymph Node Metastases	Bone Metastases	Soft Tissue Metastases
1	72	245	3.4	7 (3 + 4)	1			
2	74	352	30.0	n.a.	1			
3	73	338	80.0	n.a.	1	Innumerable lesions		1
4	57	120	40.0	7 (3 + 4)	Multifocal uptake	4		
5	69	268	13.0	7 (4 + 3)	1	1	2	
6	76	134	54.0	7 (4 + 3)	Multifocal uptake		8	
7	71	294	50.1	7 (3 + 4)	1			
8	57	268	3.2	9	2 (multifocal uptake)			
9	58	182	76.0	8	1	1	5	
10	72	283	13.7	9		No uptake		
11	75	288	200.0	7 (3 + 4)	1	26	8	1
12	60	123	15.2	9	Multifocal uptake			
13	66	304	27.0	8	1		2	
14	71	272	9.1	9	1		1	
15	66	285	25.3	7 (3 + 4)	1	2		
16	58	192	5.8	7 (4 + 3)	1			
17	69	323	37.0	7 (3 + 4)	1			
18	66	69	11.4	7 (3 + 4)	2 (multifocal uptake)			
19	65	268	7.8	9	2 (multifocal uptake)			
20	43	212	23.0	n.a.	1			
21	73	232	6.3	7 (3 + 4)	2 (multifocal uptake)			
22	84	338	16.4	9	3 (multifocal uptake)			
23	70	246	27.6	8	1			
24	74	351	12.3	9	1			

n.a. indicates not available.

Data Acquisition

The patients were intravenously administered with ^{68}Ga-PSMA-11, the ^{68}Ga-labeled HBED-CC conjugate of the PSMA-specific pharmacophore Glu-NH-CO-NH-Lys(Ahx), which was synthesized and radiolabeled as published previously (range = 69–352 MBq, median = 268 MBq).[22–24]

Data acquisition consisted of two parts: the dynamic part (dPET/CT studies) and the static part (whole-body PET/CT). dPET/CT studies were performed over the pelvic area and the lower abdomen (two bed positions, 44 cm) for 60 minutes using a 24-frame protocol (10 frames of 30 s, 5 frames of 60 s, 5 frames of 120 s, and 8 frames of 300 s). Whole-body static imaging was performed in all patients with an image duration of 2 minutes per bed position for the emission scans after the end of the dynamic acquisition. A dedicated PET/CT system (Biograph mCT, 128S; Siemens Co., Erlangen, Germany) with an axial field of view of 21.6 cm with TruePoint and TrueV, operated in a three-dimensional mode, was used. A low-dose attenuation CT (120 kV, 30 mA) was used for the attenuation correction of the dynamic emission PET data and for image fusion. A second low-dose CT from the skull to the knees (120 kV, 30 mA) was performed after the end of the dynamic series. All PET images were attenuation-corrected and an image matrix of 400 × 400 pixels was used for iterative image reconstruction. Iterative image reconstruction was based on the ordered subset expectation maximization algorithm (OSEM) with 6 iterations and 12 subsets. The reconstructed images were converted to SUV images based on the formula[25]: SUV = tissue concentration (Bq/g)/(injected dose (Bq)/body weight (g)). The SUVs 55 to 60 minutes post-injection were used for quantification of tracer data.

Data Analysis

Data analysis and evaluation was based on visual analysis of the PET/CT scans, semiquantitative evaluation based on SUV calculations, and quantitative analysis. Qualitative analysis was based on visual assessment of the PET/CT scans. Two nuclear medicine physicians (CS, ADS) evaluated the tracer accumulating areas on transaxial, coronal, and sagittal images. In particular, areas presenting with significantly enhanced ^{68}Ga-PSMA-11 uptake, apart from those in which an increased tracer uptake is considered physiological, were considered indicative for PC involvement. PC-associated lesions were classified in the following categories: primary tumors (PC), lymph node metastases, bone metastases, and soft tissue metastases.

Semiquantitative evaluation was based on volumes of interest (VOIs) and on subsequent calculation of SUV. VOIs were drawn with an isocontour mode (pseudo-snake) and were placed over the PC-associated lesions, and over regions of the prostate gland that showed no pathological tracer accumulation and, thus, served as reference.[26] SUVs were calculated in the majority of lesions. All SUVs were assessed during the whole-body/static acquisition, 80 to 90 minutes p.i. However, pelvic lesions' SUVs were calculated at two time points, at the end of the dynamic PET acquisition (55–60 min p.i.) and during the whole-body/static acquisition (80–90 min p.i.), to assess changes in tracer uptake at different time points. Lesions that were <2 mm or without clearly delineated margins were not evaluated.

The quantitative evaluation of the dynamic PET data was performed with PMOD software (PMOD Technologies Ltd., Zürich, Switzerland). It was based on irregular VOIs, drawn with an isocontour mode (pseudo-snake), placed over PC-associated lesions.[26] Time-activity curves (TACs) were created using VOIs.

Only lesions located in the anatomic area of the pelvis, where dPET/CT was performed, were evaluated quantitatively. A detailed quantitative evaluation of tracer kinetics was performed based on two-tissue compartment modeling.[27,28] The accurate measurement of the input function requires arterial blood sampling. However, it can be retrieved simplified and noninvasively from the image data with good accuracy according to methods already reported in literature and performed previously from our group.[29,30] For this reason, at least seven consecutive ROIs were placed over the common iliac artery to obtain the blood data for ^{68}Ga-PSMA-11. The recovery coefficient was 0.85 for a diameter of 8 mm. The application of two-tissue compartment modeling leads to the extraction of the parameters K_1, k_2, k_3, and k_4. In this study, the constants K_1, k_2, k_3, and k_4 were calculated taking into account the vascular fraction (V_B) in a VOI as an additional variable. The model parameters were accepted when K_1, k_2, k_3, and k_4 were <1 and V_B >0. The unit for the rate constants K_1, k_2, k_3, and k_4 is 1/min, whereas V_B is associated with the volume of blood exchanging with tissue. After compartmental analysis, we calculated the global influx (K_i) from the compartment data using the formula: $K_i = (K_1 \times k_3)/(k_2 + k_3)$. In addition to creating VOIs over foci indicative of malignant involvement, we also created VOIs over normal prostate tissue (reference tissue). The values extracted from reference tissue were then compared to the respective values of PC involvement.

Apart from compartmental analysis, a noncompartment model was used to calculate the fractal dimension (FD). FD is a parameter of heterogeneity based on chaos theory. The values of FD vary from 0 to 2 showing the deterministic or chaotic biodistribution of the ^{68}Ga-PSMA-11 activity over time.[31]

Data were statistically evaluated using the STATA/SE 12.1 (StataCorp) software on an Intel Core (2·3.06 GHz, 4 GB RAM) running with Mac OS X 10.8.4 (Apple Inc., Cupertino, CA). The statistical evaluation was performed using descriptive statistics, box plots, Wilcoxon rank-sum test, and Spearman rank correlation analysis. The results were considered significant for P less than 0.05 ($P < 0.05$).

RESULTS

Whole-Body PET/CT Studies

Visual Evaluation

In 23/24 patients, at least one PC-associated lesion was detected, leading to a detection rate of 95.8% (Figs. 1 and 2). Normal radiotracer biodistribution was demonstrated in the lacrimal

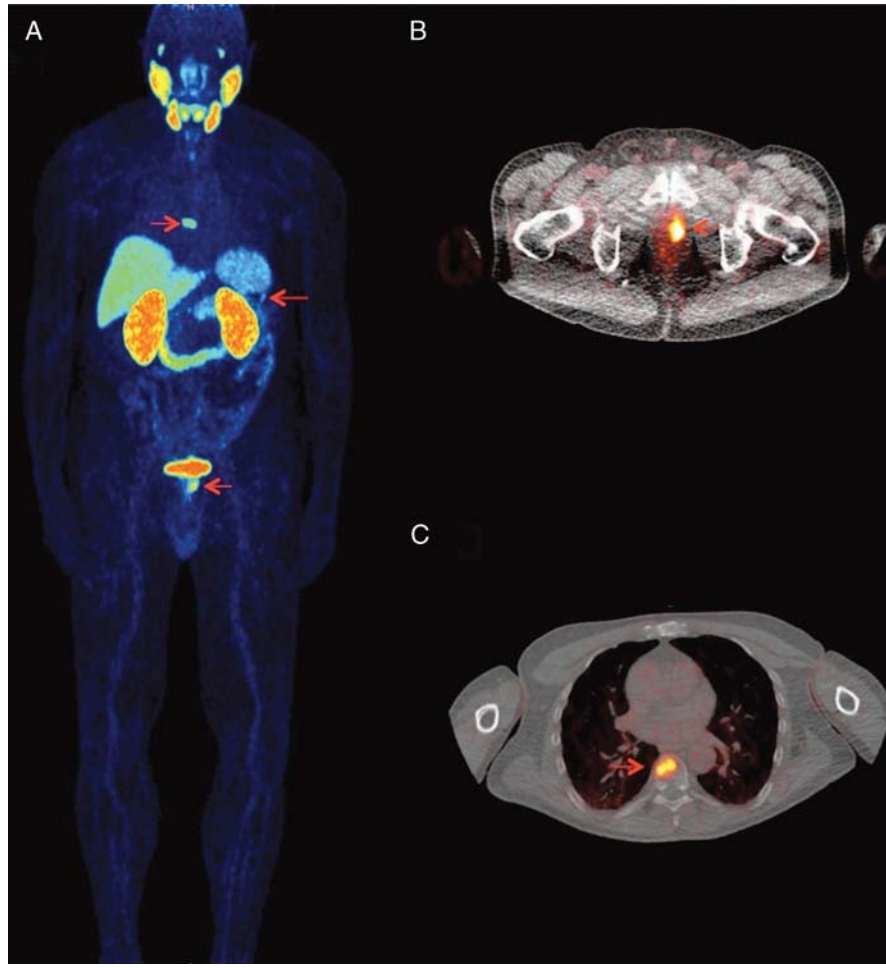

FIGURE 1. ^{68}Ga-PSMA-11 PET/CT of a 66-year-old PC patient with a PSA of 27 ng/mL. Whole-body maximum intensity projection (MIP) (**A**) reveals the primary tumor (arrow) and two skeletal metastases in the 9th thoracic vertebra and 7th left rib (arrows). Normal biodistribution of the tracer in lacrimal glands, salivary glands, nasal mucosa, liver, spleen, bowel, kidneys, and bladder. Transaxial PET/CT at the pelvic level (**B**) shows the primary tumor in the left prostate lobe (arrow). Transaxial PET/CT at the thoracic level (**C**) shows the osseous metastasis in the 9th thoracic vertebra (arrow).

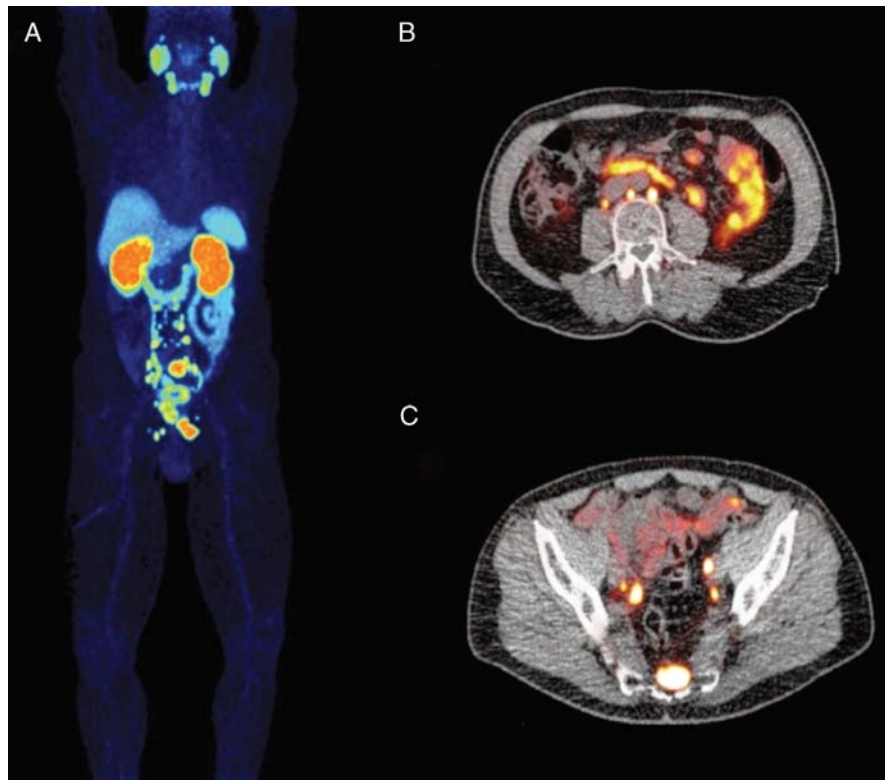

FIGURE 2. ^{68}Ga-PSMA-11 PET/CT of a 75-year-old PC patient. Whole-body maximum intensity projection (MIP) (**A**) reveals the primary tumor, and multiple lymph node and skeletal metastases. Transaxial PET/CT at the lumbar spine level (**B**) shows three retroperitoneal metastases. Transaxial PET/CT at the level of os sacrum (**C**) shows multiple iliacal lymph node metastases and infiltration of the os sacrum.

glands, salivary glands, nasal mucosa, liver, spleen, bowel, kidneys, and bladder. One patient demonstrated tracer uptake neither in PC-associated lesions nor in tissues, where physiological uptake is expected. Eight patients demonstrated multifocal tracer uptake in the prostate gland, in three of which the precise number of PC lesions could not be calculated. In one patient, the extent of lymph node and bone metastatic involvement was very large, rendering the exact calculation of metastatic osseous and lymph node metastases practically impossible. Metastatic disease was detected in nine patients, and five of them had already been examined with conventional imaging modalities (CT and/or MRI) before the ^{68}Ga-PSMA-11 PET/CT. Four of these five pre-examined subjects were positive for metastases based on conventional imaging, whereas one was negative. Interestingly, in this subgroup of 5 patients, only 4 of the total 19 ^{68}Ga-PSMA-11-positive metastatic lesions were depicted in the conventional modalities. A total of 88 PC-associated lesions were evaluated. In particular, 26 lesions corresponded to primary prostatic tumors, 34 to lymph node metastases, 26 to bone metastases, and 2 to soft tissue metastases (Table 1).

Semiquantitative Evaluation

A total of 72 of the 88 lesions were semiquantitatively (SUV) evaluated. In particular, SUVs were calculated for 26 primary prostatic tumors, 16 lymph node metastases, and 30 bone metastases (Fig. 3). According to Wilcoxon rank-sum test, lesions' SUVs were significantly higher than respective values derived from reference prostate gland. Spearman rank correlation analysis showed that PSA levels correlated significantly with PC-associated lesions' $SUV_{average}$ ($r = 0.60$, $P < 0.0001$) and SUV_{max} ($r = 0.57$, $P < 0.0001$). Moreover, a weak but significant correlation was demonstrated between Gleason score and $SUV_{average}$ ($r = 0.33$, $P < 0.05$) and SUV_{max} ($r = 0.28$, $P < 0.05$).

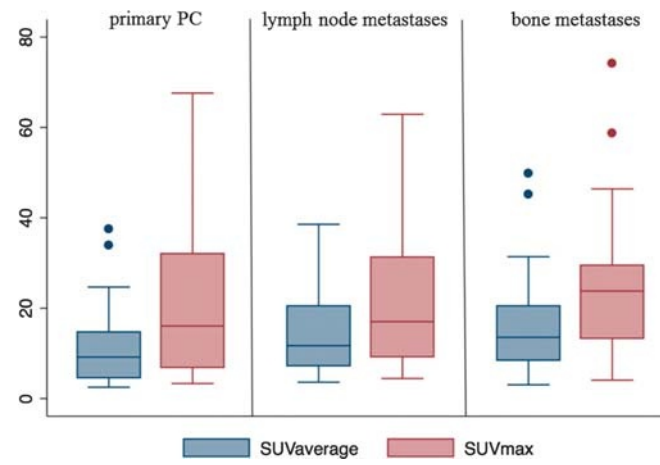

FIGURE 3. Box plots of SUVs derived from primary PC lesions (left row), lymph node metastases (middle row), and osseous metastases (right row). No statistically significant differences are depicted between different sites of PC involvement ($P < 0.05$). SUV has no unit.

Dynamic PET/CT Studies of the Pelvis

Fifty-eight ^{68}Ga-PSMA-11 pelvic lesions were quantitatively evaluated by means of dPET/CT (26 primary tumors, 13 lymph node metastases, and 19 osseous metastases). The values of SUVs and kinetic parameters derived from PC-associated lesions and from reference prostate gland are depicted in Table 2. Wilcoxon rank-sum revealed that, besides $SUV_{average}$ and SUV_{max}, the parameters k_3, influx, V_B, and FD were significantly higher in PC-related lesions than in reference tissue. Regarding the different PC recurrence sites, Wilcoxon rank-sum test revealed that osseous metastatic lesions had higher FD values than primary tumors and lymph node metastases. Furthermore, k_3 from osseous lesions was higher than k_3 from lymph node metastases ($P < 0.05$) (Fig. 4). No significant correlations were observed between kinetic parameters and PSA or Gleason score.

Moreover, we calculated the SUVs of the pelvic lesions at two time points: at the end of the dynamic PET acquisition (55–60 min p.i.; "early" SUVs) and during the whole-body/static acquisition (80–90 min p.i.; "late" SUVs). This evaluation revealed that both $SUV_{average}$ and SUV_{max} increased at late acquisition times. In particular, the mean value of "early" $SUV_{average}$ was 14.9 (median = 12.4), whereas the mean value of "late" $SUV_{average}$ was 17.8 (median = 15.8). Respectively, the mean value of "early" SUV_{max} was 24.4 (median = 19.6), whereas the mean value of "late" SUV_{max} was 29.0 (median = 24.5).

Dynamic PET/CT scanning led also to the extraction of time-activity curves (TACs), which show the activity concentration of ^{68}Ga-PSMA-11 in the selected VOI during the 60 minutes of dPET/CT acquisition. Figure 5 demonstrates the resulting TACs derived from a primary tumor, an osseous metastasis, a lymph node metastasis, and reference prostate tissue. The curves show that ^{68}Ga-PSMA-11 concentration increases in the PC-associated lesions in comparison to normal prostate.

TABLE 2. Descriptive Statistics of ^{68}Ga-PSMA-11 SUVs and Kinetic Parameters

	Parameters	Mean	Median	Minimum	Maximum
PC lesions	$SUV_{average}$*	14.3	11.8	2.5	49.8
	SUV_{max}*	23.4	19.1	3.3	74.1
	K_1 (1/min)	0.24	0.17	0.03	0.89
	k_2 (1/min)	0.21	0.14	6.8e–100	0.99
	k_3* (1/min)	0.34	0.28	0.01	0.99
	k_4 (1/min)	0.05	0.02	5.87e–99	0.91
	Influx* (1/min)	0.15	0.09	0.02	0.77
	V_B*	0.02	0.005	8.99e–08	0.17
	FD*	1.27	1.31	1.06	1.36
Reference	$SUV_{average}$	1.6	1.5	0.23	3.0
	SUV_{max}	2.2	2.4	0.6	4.0
	K_1 (1/min)	0.15	0.12	0.04	0.27
	k_2 (1/min)	0.28	0.22	0.06	0.56
	k_3 (1/min)	0.11	0.12	0.04	0.18
	k_4* (1/min)	0.1	0.07	0.4	0.32
	Influx (1/min)	0.04	0.05	0.1	0.06
	V_B	0.02	0.002	0.0001	0.1
	FD	1.02	1.06	0.06	1.15

The SUVs are derived from the 72 lesions, which were evaluated. The kinetic parameters are derived after application of two-tissue compartment modeling in the -dPET/CT data from the pelvis (58 lesions). The values of parameters K_1, k_2, k_3, k_4, and influx are 1/min. SUV, V_B, and FD have no unit.

*Significant probabilities ($P < 0.05$).

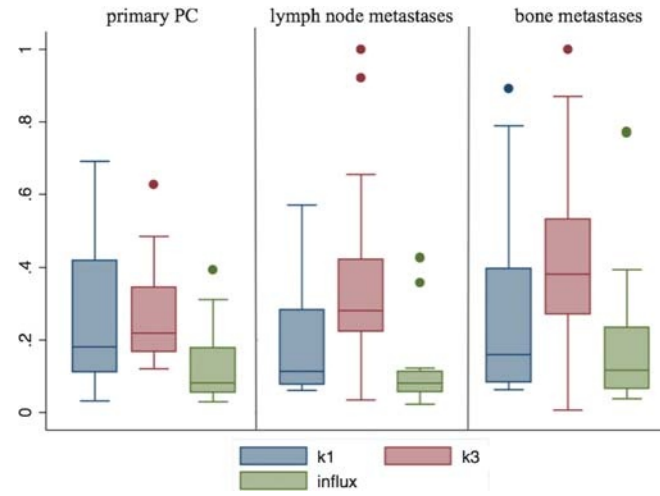

FIGURE 4. Box plots of parameters K_1, k_3, and influx derived from primary PC lesions (left row), lymph node metastases (middle row), and osseous metastases (right row). k_3 from osseous metastases is significantly higher than k_3 from lymph node metastases ($P < 0.05$). Otherwise, no other statistically significant differences are depicted between sites of PC involvement regarding these parameters. The values of parameters K_1, k_3, and influx are 1/min.

Spearman rank correlation analysis was performed between ^{68}Ga-PSMA-11 quantitative parameters. The strongest correlations ($P < 0.05$) were found between FD and $SUV_{average}$ (r = 0.93), FD and SUV_{max} (r = 0.87), FD and influx (r = 0.77), and between influx and $SUV_{average}$ (r = 0.76), influx and SUV_{max} (r = 0.75), and influx and K_1 (r = 0.82) (Table 3).

DISCUSSION

The first satisfying results from the introduction of ^{68}Ga-PSMA-11 in PC diagnostics have rendered PET imaging with this novel agent highly promising.[15–17] In this analysis, we studied the detection rate and pharmacokinetics of ^{68}Ga-PSMA-11 in a group of patients suffering from primary, histologically confirmed PC, by means of dynamic and whole-body PET/CT.

Regarding whole-body PET/CT studies, all patients but one were ^{68}Ga-PSMA-11 positive (95.8%). This high detection rate is of no surprise because the radioligand, which specifically binds to the prostate-specific membrane antigen (PSMA), is expressed practically in all PCs.[3,32,33]

Correlation analysis revealed that PSA plasma levels correlated positively with tracer uptake in PC-associated lesions, as reflected by $SUV_{average}$ (r = 0.60) and SUV_{max} (r = 0.57), a result in agreement with previous results from our group in patients with biochemical recurrence of PC.[20] Furthermore, ^{68}Ga-PSMA-11 uptake, measured by $SUV_{average}$ and SUV_{max}, correlated weak but significantly with Gleason score. This result is in line with the findings of Rowe et al., who also demonstrated a significant, positive correlation between Gleason score and SUV_{max} of the radiotracer ^{18}F-DCFBC that also targets PSMA in a group of 13 patients with primary PC.[34] A potential explanation for these weak/moderate correlations between ^{68}Ga-PSMA-11 uptake and the previously mentioned parameters could be the heterogeneity of PSMA expression in PC, also in correlation with PSA levels and Gleason score, which has been highlighted in some studies.[35,36]

Dynamic PET/CT imaging revealed that PC-associated lesions demonstrate higher ^{68}Ga-PSMA-11 uptake (SUVs), higher

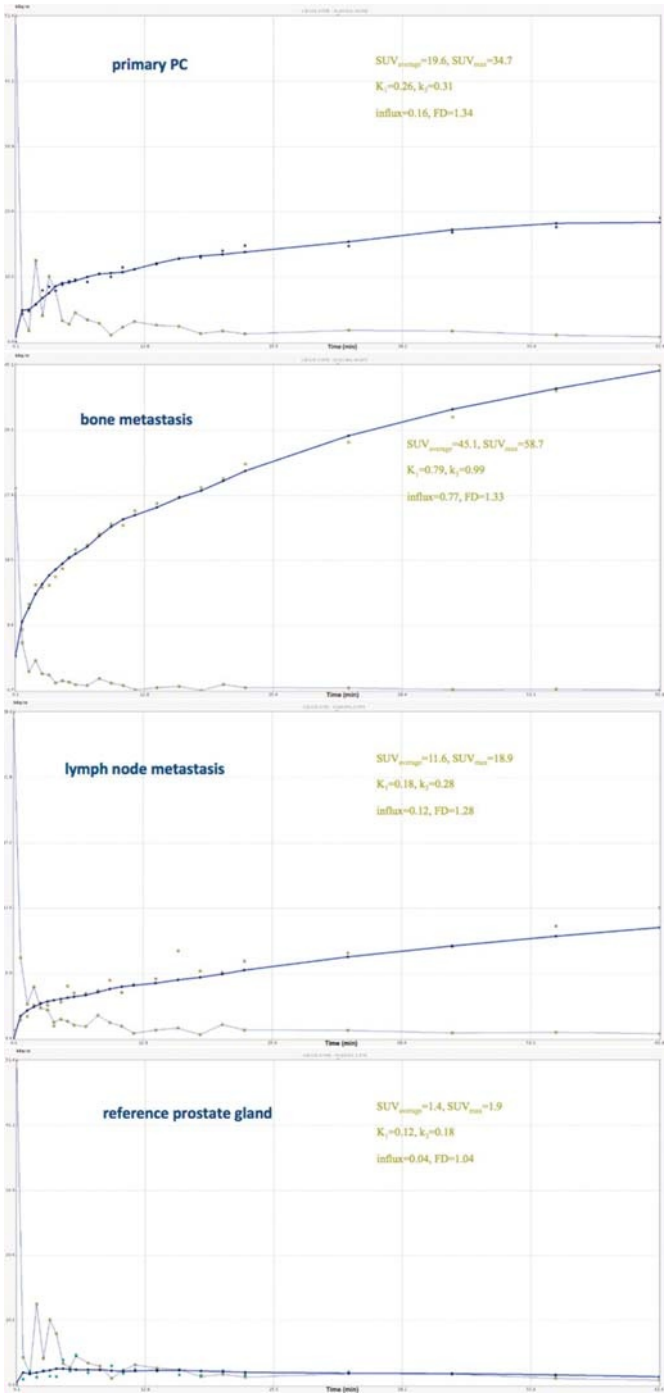

FIGURE 5. Representative time-activity curves (TACs) derived after application of two-tissue compartment modeling in the dynamic PET/CT data. The TACs are derived from VOIs drawn over a primary PC (first row), an osseous metastasis (second row), a lymph node metastasis (third row), and reference prostate gland (fourth row). The curves derived from PC-associated lesions show that ^{68}Ga-PSMA-11 accumulates increasingly in the respective VOIs in the 60 minutes of dynamic PET acquisition. On the other hand, the TAC derived from normal prostate tissue demonstrates a lower accumulation of ^{68}Ga-PSMA-11 during dynamic PET acquisition. The values of parameters K_1, k_3, and influx are 1/min. SUV and FD have no unit.

TABLE 3. Results of the Spearman Rank Correlation Analysis Between PC-Associated Lesions' Quantitative and Semiquantitative (SUVs) Parameters of ^{68}Ga-PSMA-11, Derived from dPET/CT of the Pelvis (58 Evaluated Lesions)

	$SUV_{average}$	SUV_{max}	K_1 (1/min)	k_3 (1/min)	Influx (1/min)
$SUV_{average}$					
SUV_{max}	0.9290*				
K_1 (1/min)	0.4538*	0.4757*			
k_3 (1/min)	0.6532*	0.5676*	0.010		
Influx (1/min)	0.7598*	0.7519*	0.8212*	0.3177*	
FD	0.9287*	0.8736*	0.4752*	0.5958*	0.7711*

The values of parameters K_1, k_3, and influx are 1/min. SUV and FD have no unit. Values were considered significant for $P < 0.05$.

*Significant probabilities ($P < 0.05$).

blood volume (V_B), higher forward transport rate between the reversible and trapped compartment, which is associated with higher receptor binding and internalization according to our hypothesis (k_3), and higher influx than reference prostate gland. The fact that malignant lesions demonstrate higher kinetic values than reference tissue or benign lesions has been highlighted for various tumors with different tracers.[30,37–40]

The lesions' TACs showed a steadily increasing tracer accumulation during the 60 minutes of dynamic PET acquisition (Fig. 5). Furthermore, the comparison of SUVs in the last frame of dynamic acquisition (55–60 min p.i.) and in the static/whole-body late images (80–90 min p.i.) revealed an increase of tracer uptake at late acquisition times, which has been described in a previous study even for longer time intervals.[41] The finding that ^{68}Ga-PSMA-11 shows a high receptor binding and internalization, and accumulates increasingly in the primary PC-associated lesions is in good agreement with preclinical data of the tracer[24] and previously published data from our group regarding the behavior of ^{68}Ga-PSMA-11 in pre-treated PC patients with biochemical recurrence.[20] The here presented findings confirm the previous results also in patients suffering from primary PC and imply a potential efficacy of anti-PSMA approaches in primary PC-associated lesions, especially considering the promising results of the radioligand-based anti-PSMA therapy with ^{177}Lu-PSMA-617[42] and ^{131}I-MIP-1095.[43]

This study has some limitations. Firstly, the number of patients enrolled is small. Secondly, most but not all of the ^{68}Ga-PSMA-11-positive findings on PET/CT were histopathologically confirmed. Nevertheless, the so far collected data regarding the ^{68}Ga-PSMA ligand imply that tracer-avid PET lesions with morphological correlation have to be considered as positive for PC involvement.[44] Finally, an expansion of the dynamic PET acquisition at later time points (for example at 2 h or 3 h p.i.) would provide more robust data regarding ^{68}Ga-PSMA-11 accumulation in PC-associated regions over time, a limitation partially compensated by calculating SUVs of pelvic lesions at the end of dynamic PET acquisition and during the static studies.

CONCLUSION

In the present study, the diagnostic efficacy of ^{68}Ga-PSMA-11 PET/CT in primary PC was confirmed with an overall detection rate of 95.8%. A positive correlation was demonstrated between SUVs of ^{68}Ga-PSMA-11-positive lesions and PSA plasma levels, and Gleason score. Dynamic PET/CT studies of the pelvis demonstrated that tracer uptake in PC-associated lesions is increasing

during the 60 minutes of dynamic PET acquisition. The application of two-tissue compartment modeling revealed a high receptor binding and internalization of ^{68}Ga-PSMA-11 in the PC-associated lesions.

REFERENCES

1. Pinto F, Totaro A, Palermo G, et al. Imaging in prostate cancer staging: present role and future perspectives. *Urol Int*. 2012;88:125–136.
2. Blomqvist L, Carlsson S, Gjertsson P, et al. Limited evidence for the use of imaging to detect prostate cancer: a systematic review. *Eur J Radiol*. 2014;83:1601–1606.
3. Osborne JR, Akhtar NH, Vallabhajosula S, et al. Prostate-specific membrane antigen-based imaging. *Urol Oncol*. 2013;31:144–154.
4. Lavery HJ, Brajtbord JS, Levinson AW, et al. Unnecessary imaging for the staging of low-risk prostate cancer is common. *Urology*. 2011;77:274–278.
5. Heidenreich A, Bastian PJ, Bellmunt J, et al. EAU guidelines on prostate cancer. Part 1: screening, diagnosis, and local treatment with curative intent—update 2013. *Eur Urol*. 2014;65:124–137.
6. Turkbey B, Brown AM, Sankineni S, et al. Multiparametric prostate magnetic resonance imaging in the evaluation of prostate cancer. *CA Cancer J Clin*. 2016;66:326–336.
7. Marzola MC, Chondrogiannis S, Ferretti A, et al. Role of 18F-choline PET/CT in biochemically relapsed prostate cancer after radical prostatectomy: correlation with trigger PSA, PSA velocity, PSA doubling time, and metastatic distribution. *Clin Nucl Med*. 2013;38:e26–e32.
8. Evangelista L, Zattoni F, Guttilla A, et al. Choline PET or PET/CT and biochemical relapse of prostate cancer: a systematic review and meta-analysis. *Clin Nucl Med*. 2013;38:305–314.
9. Dusing RW, Peng W, Lai SM, et al. Prostate-specific antigen and prostate-specific antigen velocity as threshold indicators in ^{11}C-acetate PET/CTAC scanning for prostate cancer recurrence. *Clin Nucl Med*. 2014;39:777–783.
10. Maurer T, Gschwend JE, Rauscher J, et al. Diagnostic efficacy of ^{68}gallium-PSMA positron emission tomography compared to conventional imaging in lymph node staging of 130 consecutive patients with intermediate to high risk prostate cancer. *J Urol*. 2016;195:1436–1443.
11. Lütje S, Heskamp S, Cornelissen AS, et al. PSMA ligands for radionuclide imaging and therapy of prostate cancer: clinical status. *Theranostics*. 2015;5:1388–1401.
12. Kosuri S, Akhtar NH, Smith M, et al. Review of salvage therapy for biochemically recurrent prostate cancer: the role of imaging and rationale for systemic salvage targeted anti-prostate-specific membrane antigen radioimmunotherapy. *Adv Urol*. 2012;2012:921674.
13. Bott SR. Management of recurrent disease after radical prostatectomy. *Prostate Cancer Prostatic Dis*. 2004;7:211–216.
14. Beer AJ, Eiber M, Souvatzoglou M, et al. Radionuclide and hybrid imaging of recurrent prostate cancer. *Lancet Oncol*. 2011;12:181–191.
15. Afshar-Oromieh A, Zechmann CM, Malcher A, et al. Comparison of PET imaging with a (68)Ga-labelled PSMA ligand and (18)F-choline-based PET/CT for the diagnosis of recurrent prostate cancer. *Eur J Nucl Med Mol Imaging*. 2014;41:11–20.
16. Afshar-Oromieh A, Avtzi E, Giesel FL, et al. The diagnostic value of PET/CT imaging with the (68)Ga-labelled PSMA ligand HBED-CC in the diagnosis of recurrent prostate cancer. *Eur J Nucl Med Mol Imaging*. 2015;42:197–209.
17. Eiber M, Maurer T, Souvatzoglou M, et al. Evaluation of hybrid 68Ga-PSMA-ligand PET/CT in 248 patients with biochemical recurrence after radical prostatectomy. *J Nucl Med*. 2015;56:668–674.
18. Silver DA, Pellicer I, Fair WR, et al. Prostate-specific membrane antigen expression in normal and malignant human tissues. *Clin Cancer Res*. 1997;3:81–85.
19. Eder M, Eisenhut M, Babich J, et al. PSMA as a target for radiolabelled small molecules. *Eur J Nucl Med Mol Imaging*. 2013;40:819–823.
20. Sachpekidis C, Eder M, Kopka K, et al. ^{68}Ga-PSMA-11 dynamic PET/CT imaging in biochemical relapse of prostate cancer. *Eur J Nucl Med Mol Imaging*. 2016;43:1288–1299.
21. Guo N, Lang L, Gao H, et al. Quantitative analysis and parametric imaging of ^{18}F-labeled monomeric and dimeric RGD peptides using compartment model. *Mol Imaging Biol*. 2012;14:743–752.
22. Eder M, Schäfer M, Bauder-Wüst U, et al. ^{68}Ga-complex lipophilicity and the targeting property of a urea-based PSMA inhibitor for PET imaging. *Bioconjug Chem*. 2012;23:688–697.
23. Eder M, Neels O, Müller M, et al. Novel preclinical and radiopharmaceutical aspects of [68Ga]Ga-PSMA-HBED-CC: a new PET tracer for imaging of prostate cancer. *Pharmaceuticals (Basel)*. 2014;7:779–796.
24. Schäfer M, Bauder-Wüst U, Leotta K, et al. A dimerized urea-based inhibitor of the prostate-specific membrane antigen for ^{68}Ga-PET imaging of prostate cancer. *EJNMMI Res*. 2012;2:23.
25. Strauss LG, Conti PS. The applications of PET in clinical oncology. *J Nucl Med*. 1991;32:623–648.
26. http://www.pmod.com/files/download/v31/doc/pbas/4729.htm.
27. Sokoloff L, Smith CB. Basic principles underlying radioisotopic methods for assay of biochemical processes in vivo. In: Greitz T, Ingvar DH, Widén L, eds. *The Metabolism of the Human Brain Studied with Positron Emission Tomography*. New York: Raven Press; 1983:123–148.
28. Miyazawa H, Osmont A, Petit-Taboué MC, et al. Determination of ^{18}F-fluoro-2-deoxy-D-glucose rate constants in the anesthetized baboon brain with dynamic positron tomography. *J Neurosci Methods*. 1993;50:263–272.
29. Ohtake T, Kosaka N, Watanabe T, et al. Noninvasive method to obtain input function for measuring tissue glucose utilization of thoracic and abdominal organs. *J Nucl Med*. 1991;32:1432–1438.
30. Strauss LG, Klippel S, Pan L, et al. Assessment of quantitative FDG PET data in primary colorectal tumours: which parameters are important with respect to tumour detection? *Eur J Nucl Med Mol Imaging*. 2007;34:868–877.
31. Dimitrakopoulou-Strauss A, Strauss LG, Burger C, et al. On the fractal nature of positron emission tomography (PET) studies. *World J Nucl Med*. 2003;4:306–313.
32. Bostwick DG, Pacelli A, Blute M, et al. Prostate specific membrane antigen expression in prostatic intraepithelial neoplasia and adenocarcinoma: a study of 184 cases. *Cancer*. 1998;82:2256–2261.
33. Tsourlakis MC, Klein F, Kluth M, et al. PSMA expression is highly homogenous in primary prostate cancer. *Appl Immunohistochem Mol Morphol*. 2015;23:449–455.
34. Rowe SP, Gage KL, Faraj SF, et al. ^{18}F-DCFBC PET/CT for PSMA-based detection and characterization of primary prostate cancer. *J Nucl Med*. 2015;56:1003–1010.
35. Mannweiler S, Amersdorfer P, Trajanoski S, et al. Heterogeneity of prostate-specific membrane antigen (PSMA) expression in prostate carcinoma with distant metastasis. *Pathol Oncol Res*. 2009;15:167–172.
36. Miyamoto DT, Sequist LV, Lee RJ. Circulating tumour cells—monitoring treatment response in prostate cancer. *Nat Rev Clin Oncol*. 2014;11:401–412.
37. Dimitrakopoulou-Strauss A, Strauss LG, Heichel T, et al. The role of quantitative (18)F-FDG PET studies for the differentiation of malignant and benign bone lesions. *J Nucl Med*. 2002;43:510–518.
38. Doot RK, Muzi M, Peterson LM, et al. Kinetic analysis of ^{18}F-fluoride PET images of breast cancer bone metastases. *J Nucl Med*. 2010;51:521–527.
39. Sachpekidis C, Goldschmidt H, Hose D, et al. PET/CT studies of multiple myeloma using (18)F-FDG and (18)F-NaF: comparison of distribution patterns and tracers' pharmacokinetics. *Eur J Nucl Med Mol Imaging*. 2014;41:1343–1353.
40. Henze M, Dimitrakopoulou-Strauss A, Milker-Zabel S, et al. Characterization of ^{68}Ga-DOTA-D-Phe1-Tyr3-octreotide kinetics in patients with meningiomas. *J Nucl Med*. 2005;46:763–769.
41. Benešová M, Schäfer M, Bauder-Wüst U, et al. Preclinical evaluation of a tailor-made DOTA-conjugated PSMA inhibitor with optimized linker moiety for imaging and endoradiotherapy of prostate cancer. *J Nucl Med*. 2015;56:914–920.
42. Kratochwil C, Giesel FL, Eder M, et al. [^{177}Lu]Lutetium-labelled PSMA ligand-induced remission in a patient with metastatic prostate cancer. *Eur J Nucl Med Mol Imaging*. 2015;42:987–988.
43. Zechmann CM, Afshar-Oromieh A, Armor T, et al. Radiation dosimetry and first therapy results with a (124)I/(131)I-labeled small molecule (MIP-1095) targeting PSMA for prostate cancer therapy. *Eur J Nucl Med Mol Imaging*. 2014;41:1280–1292.
44. Afshar-Oromieh A, Hetzheim H, Kratochwil C, et al. The theranostic PSMA-ligand PSMA-617 in the diagnosis of prostate cancer by PET/CT: biodistribution in humans, radiation dosimetry and first evaluation of tumor lesions. *J Nucl Med*. 2015;56:1697–1705.